Dynamics of guiding highly charged ions through SiO_2 nanocapillaries

H.-Q. Zhang,* P. Skog, and R. Schuch
Atomic Physics, Fysikum, Stockholm University, S-10691 Stockholm, Sweden
(Received 23 July 2010; revised manuscript received 15 September 2010; published 4 November 2010)

The time evolution of angular distributions of 7-keV Ne^{7+} ions transmitted through SiO_2 nanocapillaries is studied starting with already-charged capillaries, as well as with fully discharged capillaries, under well-defined conditions. We deduce the rearrangement of charge patches for the charged capillaries from the time evolution of the angular distributions. The rearrangement time is found to be orders of magnitude shorter than the discharge time. Combined with a model calculation, we derive quantitative information on the formation of charge patches downstream of the entrance patch during charging-up, starting with the fully discharged capillaries. A pattern of a small number of charge patches guiding ions is deduced in the stationary state of transmission. The model predicts the width and broadening of the transmitted intensity in accord with measurements. We find strong evidence that the deposited charge patches, formed during charge-up, remain localized in the steady state of ion transmission.

DOI: 10.1103/PhysRevA.82.052901 PACS number(s): 61.85.+p, 34.50.−s

I. INTRODUCTION

Interaction of highly charged ions (HCIs) with nanocapillaries has received considerable attention in the past few years. Earlier work on HCIs transmitted through metallic nanocapillaries pertained to the study of hollow atom formation [1–4]. With metallic nanocapillaries, it was found that HCIs are transmitted only at tilt angles limited by the capillary aspect ratio. However, with insulating nanocapillaries, transmission of HCIs has been observed even when the capillary membranes are tilted by an angle larger than the angle given by the aspect ratio [5–11]. It has been found that the angular distributions of transmitted ions were centered around the direction of the capillary axes and that the majority of transmitted ions retain their initial charge state and kinetic energy. This guiding effect of HCIs through insulating nanocapillaries shows that it is possible to bend a beam of slow HCIs by a few degrees [5–11]. The ion-guiding of single tapered glass capillaries has been used to produce a microbeam of HCIs [12], which can be used for controlled surface modification [13] or to selectively damage the different constituents of biological cells [14]. The study of HCIs guiding through insulating nanocapillaries also provide means to probe the electrical properties of insulating nanocapillaries, i.e., the charge-up properties of insulators and transport of charges in bulk and surface.

The guiding of HCIs through nanocapillaries in insulating materials has been attributed to a self-organized arrangement of charge patches on the inner walls of the capillaries [5–22]. The nonconducting inner surface of the nanocapillaries collects charges due to ion impact. A charge patch can be formed at the entrance region, which is exposed to direct impact of incident ions. Downstream of this first patch, additional charge patches may also be formed. Simulations for nanocapillaries in *polyethylene terephthalate* (PET) [11] show a double peak structure in the transmitted angular distribution due to the existence of another charge patch. However, such a double peak structure has so far not been observed, instead, recent experimental studies showed that the transmitted angular distribution shifts by the sequentially formed charge patches [16]. This behavior was found with different capillary materials [16–18].

We reported sequential formation of three charge patches for steady-state transmission of ions through nanocapillaries with given parameters [16]. In this work, more evidence for this, as well as for the number of localized patches, is given by studying the time evolution of the transmitted angular distributions under defined conditions: already-charged, as well as fully discharged, capillaries. We will interpret the results quantitatively by a model calculation of charge-up, starting with a fully discharged capillary membrane. Stolterfoht *et al.* [18] suggest that additional charge patches downstream of the entrance patch will lose their significance in the stationary state of transmission. We show evidence for a stable charge pattern of a small number of charge patches, guiding ions in the stationary state of transmission. For the already-charged capillaries, the rearrangement of charge patches is deduced from the time evolution of the angular distributions.

II. EXPERIMENTS

The experiments were performed using the 14.5-GHz ECR ion source at the Manne Siegbahn Laboratory in Stockholm. A beam of 7-keV Ne^{7+} ions was analyzed with a bending magnet, focused by an electrostatic lens system, and collimated to a size of 2×2 mm^2 with an intensity ranging from 10 to 90 pA. A two-dimensional (2D) micro channel plate (MCP) detector of 45 mm in diameter with a resistive anode was mounted to record transmitted ions at a distance of 617 mm beyond the target position. The processed signals from the ions hitting the detector were registered by a data acquisition system in event mode. A registered event contains the 2D position information and time of impact on the detector, as well as the accumulated incident charge on the capillary membrane. The base pressure in the experimental chamber was maintained at $\approx 2.0 \times 10^{-8}$ mbar.

In the experiments, the capillary membrane can be oriented perpendicularly to the incident beam by two angles: tilt angle and elevation angle. The angle between the capillary axes

*zhanghq@physto.se or zhanghq02@gmail.com

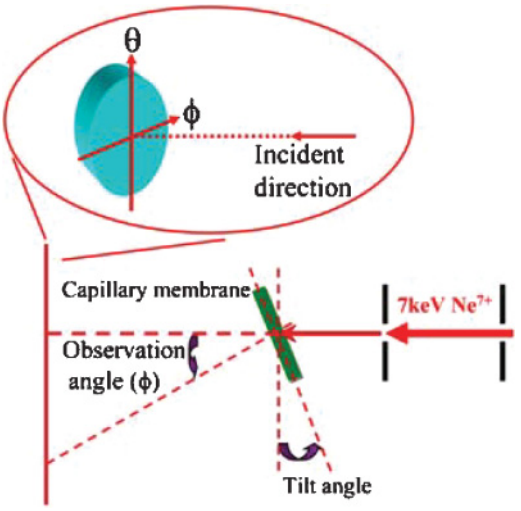

FIG. 1. (Color online) Schematic of the experimental setup. The tilt angle denotes the angle between the capillary axes and the incident beam. The observation angle is given with respect to the incident beam.

and the incident beam is referred to as the tilt angle and the elevation angle lies in a plane perpendicular to this. The observation angles ϕ and θ are given with respect to the incident beam direction. The angle ϕ lies in the same plane as the tilt angle, and the angle θ lies in a plane perpendicular to this plane. The tilt angle and observation angles are shown in Fig. 1. We aligned the capillaries to the incident beam by scanning tilt angle and elevation angle for the maximum transmission. The alignment of the capillaries is also confirmed by the agreement of the peak center of the transmitted angular distribution with that of the incident beam profile. The incident beam was imaged by the 2D MCP detector as shown in Fig. 2. This beam profile was obtained with lower beam current by

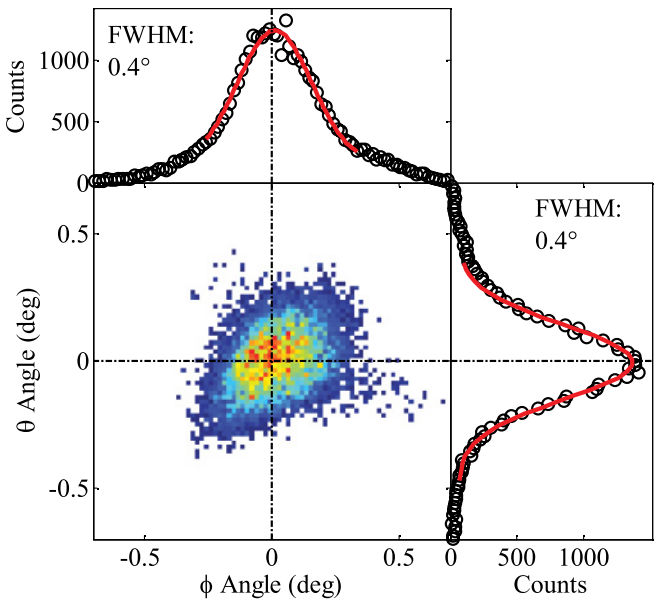

FIG. 2. (Color online) The incident beam (7-keV Ne^{7+}) image and corresponding projections on the ϕ plane (top) and θ plane (right) (see text). The solid lines in the projections are Gaussian fit curves.

reducing the focusing of the electrostatic lens system close to the ion source, far from the fixed collimation slits, since the detector would saturate at high count rate. The divergence of the beam was measured to be less than 0.4° (full width at half maximum, FWHM).

The membrane used in the experiments contains capillaries with diameters of 100 nm and lengths of 25 μm. The geometrical opening angle of the capillaries, as given by the aspect ratio, is 0.23°. The surfaces of the capillary membrane were covered by 30-nm-thick gold layers to prevent them from charging up. The geometrical transparency is 0.4%, with an intercapillary distance of 1.4 μm and the density of capillaries is 5×10^7 cm^{-2}. Details of the capillary membrane can be found in previous work [19].

III. RESULTS

A. Charged capillaries

During alignment, the capillaries are being charged up. When the tilt angle of the capillaries is changed, the established charge patches from the previous tilt angle affects the formation of new patches at the changed tilt angle. Here we show this memory effect in a defined initial condition by having the capillaries charged up to the steady state of transmission at a tilt angle of +2°. Then the tilt angle was changed to +1° in order to study the rearrangement of charge patches. Projections of the angular distributions in the ϕ plane at the tilt angle +1° as a function of the incident charge per capillary (e/capillary) are shown in Fig. 3. A double peak structure in the angular distribution was observed after the rotation; the first peak is centered around +1°, while the second peak is centered around +2°. The first peak grows and shifts toward the beam direction and in the later stage it shifts back to the orientation of the capillary axes. The second peak merges with the first peak as the transmission reaches the stationary state again. The angular width, the FWHM, is ≈1° for the tilt angle +1° at the stationary state of transmission. The evolution of transmitted angular distributions at the changed tilt angle comes from the rearrangement of charge patches inside the capillaries. The real time for the rearrangement, i.e., the time for reaching the steady state is here around 2000 s. This is in the order of charge-up time and much shorter than the typical discharge time.

B. Discharged capillaries

For a measurement with initially completely discharged capillaries, the membrane was oriented at a tilt angle of −2° and then discharged for days. Also after letting the membrane discharge for 3 months, while keeping all the settings for the beam alignment and the capillary orientation, the charging-up measurement gave the same results.

In the left column of Fig. 4, the time evolution of transmitted angular distributions projected onto the ϕ plane is shown for the charge-up process. In the middle column of Fig. 4 we show a plot of the center positions of the angular distributions in the ϕ plane as a function of incident charge per capillary (scale on the right ordinate). Starting from completely discharged capillaries, it is obvious that the angular distribution oscillates back and forth, initially from ≈−1.4°, passing the tilt angle −2°, and reaching *a turning point* at ≈−2.2°, where it shifts

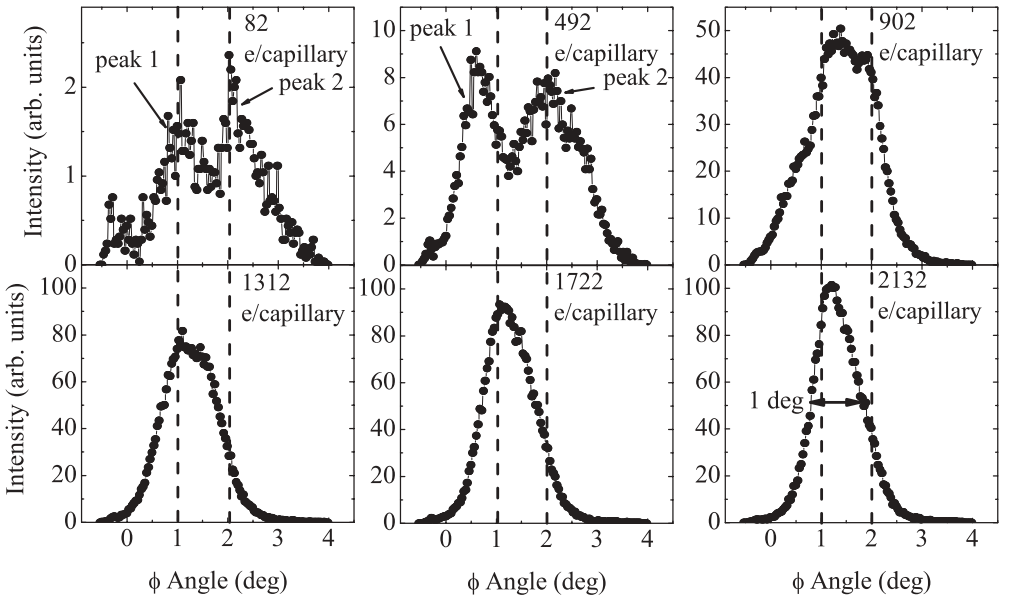

FIG. 3. Transmitted angular distributions in the ϕ plane for various amounts of accumulated incident charge in units of elementary charge per single capillary (e/capillary) at tilt angle $+1^\circ$, after rotating from $+2^\circ$. Dashed lines indicate $+1^\circ$ and $+2^\circ$, respectively.

gradually back to the tilt angle. The time evolution of the angular width (FWHM) in the ϕ plane is shown in the right column of Fig. 4 for the charge-up process. The FWHM is around 0.6° in the beginning and broadens to 0.9° in the stationary state. In the θ plane, it is found that the center of the angular distributions remains fixed within 0.15° in comparison to the larger movement in the ϕ plane and that the FWHM lies constantly around $0.9^\circ \pm 0.1^\circ$.

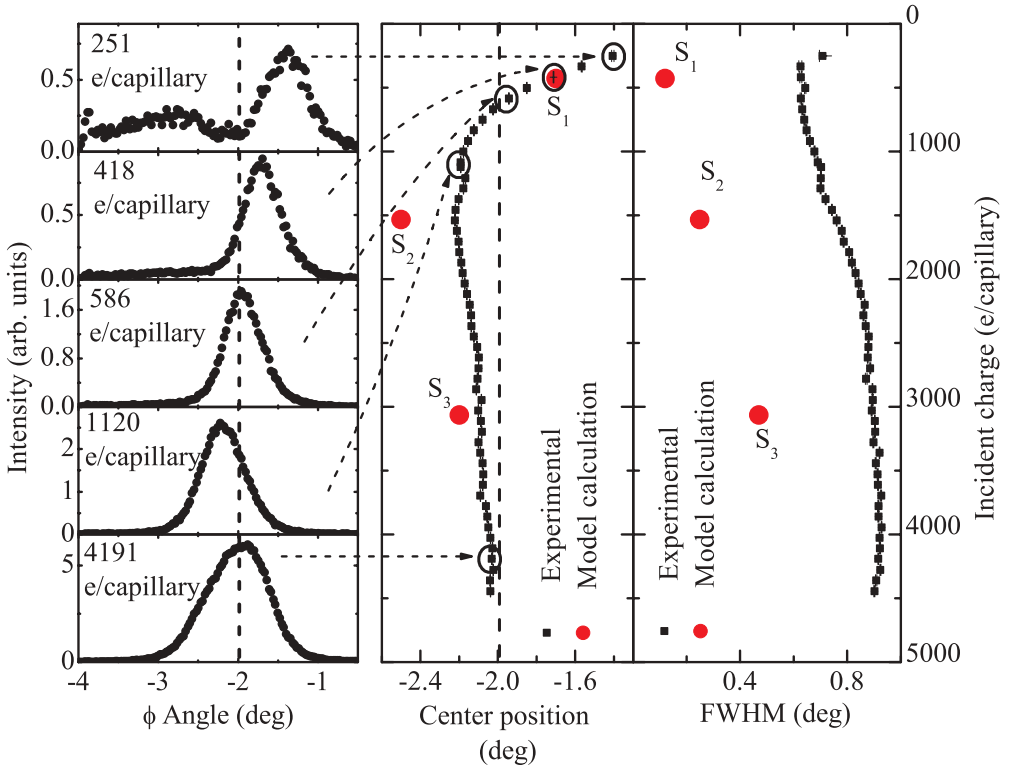

FIG. 4. (Color online) Time evolution of transmitted angular distributions at tilt angle -2° for initially discharged capillaries. (Left) Projections onto the ϕ plane for certain amounts of accumulated incident charge; (middle) peak centers (dashed lines, arrows, and circles connect the peak centers to projections); (right) FWHM. The results from model calculations are also indicated by S_1, S_2, and S_3 for different stages of charge-up (see Sec. IV).

IV. INTERPRETATION AND DISCUSSION OF RESULTS

A. Model calculation for initially discharged capillaries

For a complete understanding of observed phenomena, it would be valuable to perform an *ab initio* calculation; however, this is still out of reach [11,23]. In order to quantitatively interpret the observations, we have performed a model calculation that will be described here in detail. A brief description of it for the fully discharged capillaries was reported in our earlier work [16]. Starting from fully discharged nanocapillaries, the aim of the model calculation is to derive the patterns of the charge patches related to the observed shifts and broadenings of the angular distributions. These originate from the fields or potentials due to the charge patches.

The model calculation starts from an assumed model potential as follows [16]:

$$U_{z\rho\varphi} = U_z U_\rho U_\varphi = U_z\, e^{-(a-\rho)/a} \cos^n\left(\frac{\varphi+\varphi_0}{2}\right). \quad (1)$$

Here U_z is an adjustable parameter to model the charge density on the inner surface of capillary along the axial direction (z direction, coordinates as given in Fig. 5). The radial component of the model potential from the charge patch is assumed to be an exponential decay function similar to the modified planar potential component, where a is the radius of the capillary and ρ is the radial displacement of an ion from the center of the capillary. The cosine power function is a modified version of a $\cos^2$-like function as suggested in Ref. [5] for the φ-dependent part of the model potential. The parameter φ_0 is the angle for the potential reaching the maximum value in the angular direction, corresponding to the maximum value of the charge density. The exponent n is a parameter which is used to differentiate the cases when the charge patch is more (or less) concentrated in the φ direction. The φ-dependent part of the model potential originates from the charge deposition at the entrance. The direct impact of ions at the entrance will give an anisotropic charge deposition in the φ direction in cylindrical coordinates [5]. If ions enter a capillary in the direction parallel to the xz plane, the deposited charge density on the inner surface of the capillary at the entrance will give a maximum value in the xz plane ($\varphi = 0$ or π) (see Fig. 5). Therefore, the deflection from the charge patch creates an angular spread in the plane perpendicular to the plane of incidence. For example, ions entering in the xz plane ($\varphi = 0$ or π) introduce an angular spread in the yz plane ($\varphi = \pm\pi/2$). Note that this feature is taken into account by the φ-dependent part of the model potential, which may deflect ions and give an angular spread in the plane perpendicular to the incidence plane.

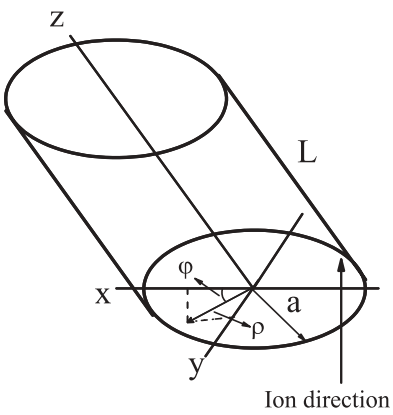

FIG. 5. Geometry used in the model calculation (see Sec. IV A).

In the model potential, the terms U_z and U_φ account for the possible charge distribution on the inner surface of the capillary. In the model calculation, we divide the capillary into short cylindrical regions and assign the potential, U_z, values in the places where the charge patches are formed. A higher value of U_z reflects a higher charge accumulation on the surface [21,22]. The limit of U_z depends on the electrical properties of the capillaries. The largest value of U_z should be limited by the dc dielectric break down strength of the capillary material (in the order of 10 MV/cm for SiO_2 [24]). The capillary membrane utilized in the measurements was thermally oxidized to grow a 100-nm-thick layer of silicon dioxide on the Si capillary walls. This sets the upper limit of U_z to 100 V. The initial value of U_z at the entrance region is chosen larger than the transverse energy of the ions so they are deflected. When the ions enter the capillary at $\rho = 0$, their maximum transverse energy can be approximated by $(1 - 1/e)U_z|_{\text{entrance}}q$ from the radial part of the model potential [see Eq. (1)], where $U_z|_{\text{entrance}}$ is the value of U_z at the entrance region and q is the charge state of incident ions. The final U_z value and distribution of charge patches are obtained when the center of the resulting angular distribution and the transmission rate are close to the experimental finding. The ion trajectories can be calculated from Newton's equation of motion under the model potential. A Monte Carlo method was used, and the beam divergence was taken into account during initialization of the ions' positions and velocities.

B. Comparison of model calculation with experimental results

As ions enter initially discharged capillaries, their direct impact at the entrance will form a charge patch. In the case of the tilt angle of -2°, the entrance patch covers about the first tenth of the capillary length. The aspect ratio for the remaining 9/10 of the capillary length is then 225:1, which allows an exit angle interval of $\approx 0.26^\circ$. The entrance patch may deflect some later incident ions toward the downstream regions to form a second patch [Fig. 6(a)]. This second patch facilitates transmission at a smaller deflection angle, $\approx -1.4^\circ$, i.e., closer to the incident beam direction, in the beginning of charging-up (incident charge $\leqslant 250\ e$/capillary). The second patch is not as localized as the entrance patch in the angular direction (φ direction) due to the preceding deflections introducing a spread in the plane perpendicular to the plane of incidence. Therefore, $n = 1$ was inserted in U_φ for the second patch. Hence, in the early stage of charging-up (incident charge $\leqslant 250\ e$/capillary), denoted S_1, we have a charge pattern with two patches, one located at the entrance with $\varphi_0 = -\pi$ and $n = 2$ set in U_φ and the other at $\varphi_0 = 0$ and $n = 1$ set in U_φ around the middle of the capillary. The value of U_z in this stage, S_1, is $\sim$3 V for the entrance patch and $\sim$0.25 V for the second patch. U_z at the entrance patch has an order of magnitude larger value than that for the second patch. This agrees with the transverse energy difference between the ions passing the

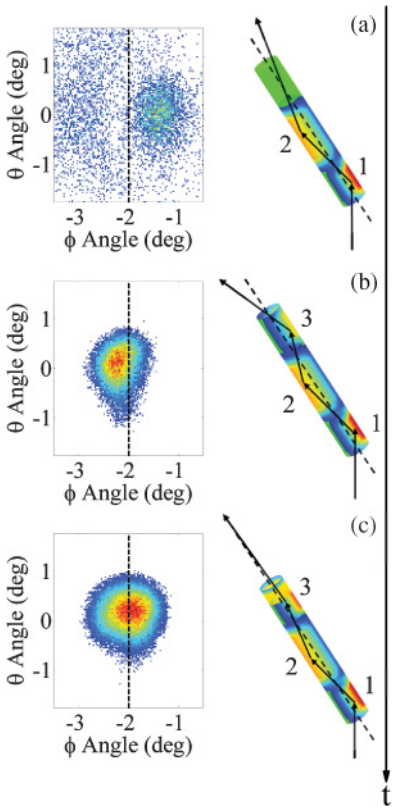

FIG. 6. (Color online) The two-dimensional angular distributions from experiment (left, with tilt angle indicated by dashed lines) and schematic drawings of charge patches (right) at different stages (a), (b), and (c) during charging-up at the tilt angle -2° (see Sec. IV B).

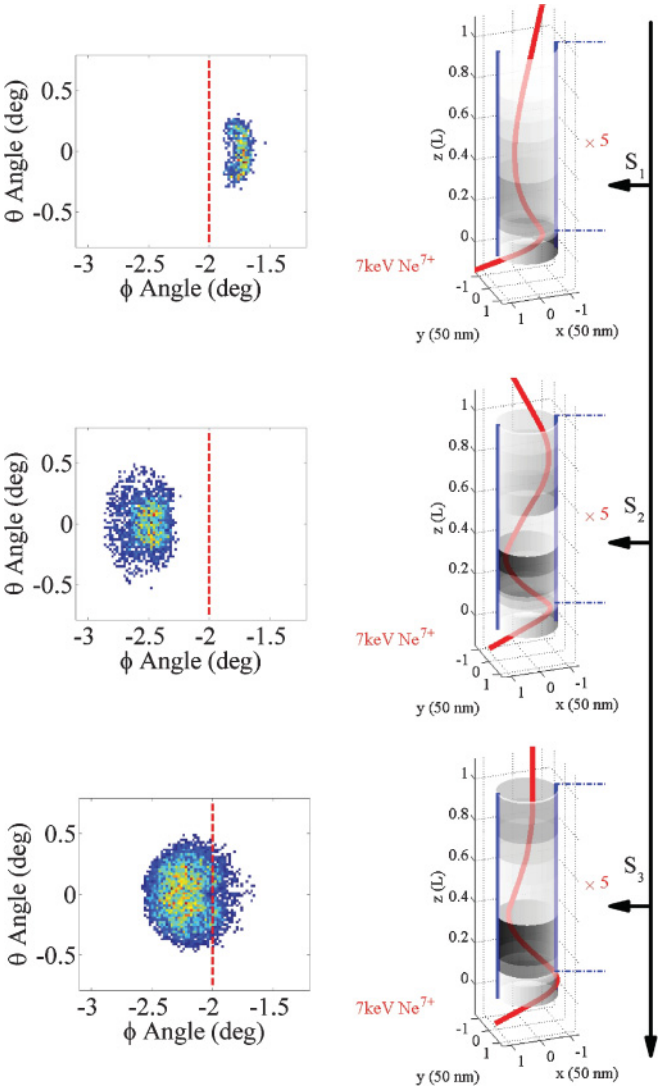

FIG. 7. (Color online) The calculated two-dimensional angular distributions (left) and corresponding distributions of charge patches on the inner surface of a capillary for three stages of the charging-up process: S_1, the early stage; S_2, around the turning point; S_3, the stationary state. Typical trajectories from the model calculations are also shown in the graph to the right. The tilt angle of the capillary is indicated by dashed lines in the graphs (left). The density of charge downstream of the entrance patch was enlarged by a factor of 5 for visibility.

entrance and the ions moving inside the capillary after the entrance. Also, the derived charge pattern is approximated by deposited charges due to ion impacts in the trajectory calculation. The calculated angular distributions are shown in Fig. 7 (left). The derived charge patterns on the inner surface of the capillary are also shown in Fig. 7 (right).

After the formation of the second patch in stage S_1, some of the ions undergo deflections from the entrance patch and the second patch. They continue further toward the exit. These ions may build up another charge patch near the capillary exit [Fig. 6(b)]. Therefore, in the stage around the turning point denoted by S_2, a charge pattern, with three charge patches located on alternating sides of the capillary walls in the plane of incidence, are placed in the capillary. For the charge patch at the exit, $n = 1$ and $\varphi_0 = -\pi$ was set in U_φ. In order to account for the draining of the deposited charges, U_z values for the entrance patch and second patch are reduced to smaller values in stage S_2 compared to stage S_1. The final U_z values were obtained when the derived charge pattern is approximated by deposited charges due to ion impacts in the trajectory calculation. The calculated transmission image in stage S_2 shifts to the left [see Fig. 7 (left)] compared with the early stage S_1, toward larger deflection angles until a turning point is reached (Fig. 4). The projections of the calculated distributions onto the ϕ plane (Fig. 8) show that the angular width in stage S_2 is larger than that in the earlier stage S_1. It is mainly due to the reduction in collimation by the exit patch.

With increasing collected charge, the transmitted angular distribution shifts back toward the tilt angle [Fig. 6(c)]. This is due to that the exit patch becomes more extended around the circumference of the capillary. Consequently, in the stationary state, S_3, a charge pattern with a change of U_φ with φ_0 from 0 to $\pm\pi/2$ at the last part of the exit patch was set. U_φ at the last part of the exit patch is then the sum of the potentials with $\varphi_0 = +\pi/2$ and $-\pi/2$ and $n = 2$ is used for both cases. As shown both in Figs. 7 and in 8, the calculated angular distribution shifts back toward the tilt angle compared to that in the stage S_2. The calculated angular distribution in the ϕ plane is also broadened (see Fig. 8) by changing the preferential charge deposition to the θ plane ($\varphi_0 = \pm\pi/2$) in the last part

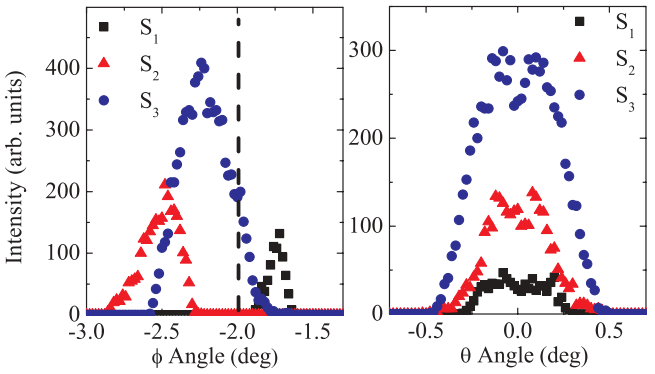

FIG. 8. (Color online) Projections of the transmitted angular distributions [(left) projections onto the ϕ plane, (right) projections onto the θ plane] from the model calculation for 7-keV Ne^{7+} transmission through SiO_2 nanocapillaries at the tilt angle -2°. Different stages of charge-up are indicated by S_1, S_2, and S_3 (see Sec. IV B). The tilt angle of the capillary is indicated by a dashed line in the left graph.

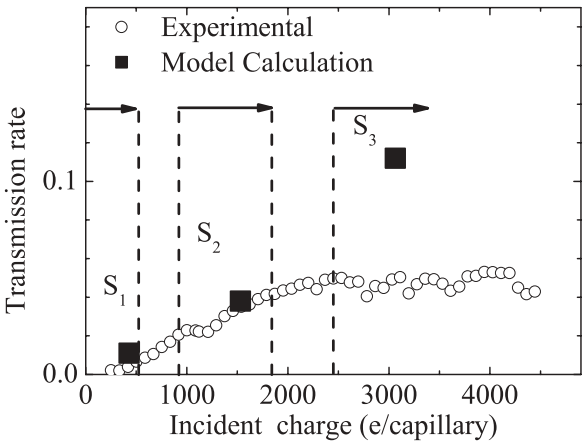

FIG. 9. Transmission rates from the model calculations are shown together with experimental rates during charging-up for the tilt angle -2°. Different stages, for which calculations were performed, during charging-up are indicated by S_1, S_2, and S_3 (see Sec. IV B).

of the exit patch which in turn adds an angular spread in the ϕ plane ($\varphi_0 = 0$).

The center position and the width of the projections onto the ϕ plane from the model calculation are plotted together with the experimental values in Fig. 4 for the three different stages of charge-up. Although the peak centers differ slightly from the experimental peak centers, the shift is reproduced reasonably well (see Fig. 4). The angular width increases in the ϕ plane while, in the θ plane, the angular width does not vary so much (Fig. 8), which is in good agreement with the experiments. However, the calculated angular widths are smaller than the experimental widths (see Fig. 4). This difference is, however, acceptable, regarding the simplicity of the model calculation. Only one representative capillary was used in the calculation while in the experiment in the order of 10^6 capillaries contribute to the transmitted angular distribution. Accounting for a small but, not completely negligible, spread of the capillary axes ($<0.2^\circ$) already gives a better agreement. Furthermore, charge fluctuations in the patches were not included in the model calculation. The calculated transmission rate, plotted together with the experimental transmission rate in Fig. 9, confirms the consistency of the model calculations.

C. Initially discharged capillaries: Shift of transmitted angular distributions

The time evolution of the transmitted angular distributions that is observed in our work is similar to that seen by others [17,18] concerning the oscillating shifts. The shifts are outside the range of the angular limits given by the aspect ratio, which implies that charge patches are formed downstream of the entrance patch. However, two main differences between our results and those from Kanai *et al.* [17] and Stolterfoht *et al.* [18] are found. One is the observation of the transmission from the deflections at the entrance patch in the very beginning of charging-up. The other is the significance and number of the charge patches downstream of the entrance patch in the stationary state of transmission.

1. The initial deflection at the entrance charge patch

In the beginning of charging-up, the entrance patch may deflect some later incident ions toward the downstream regions and also some of these ions can be directed toward the exit. This leads to two possible scenarios: the ions hit the wall and form a second patch as described in the model calculation or the ions exit from the capillaries. We examine the case in which ions exit from the capillaries. The evolution of the entrance charge patch would only allow the center of the distribution to shift within the range from -2° tilt angle to a larger deflection angle -2.26° (see Figs. 1 and 4). We checked our data from the very beginning of charge-up process; however, no transmitted intensity was visible at the allowed angles. This may be attributed to a small solid angle from the high aspect ratio we have here and a very short time until the second charge patch is established. We note that in the experiments of Kanai *et al.* [17], for 7-keV Ne^{7+} at tilt angle 2.8°, they also did not observe transmission at angles expected from deflection at the first patch, i.e., between angles of 2.8° to 4.2°. However, for somewhat lower Ne^{7+} energies, Kanai *et al.* [17] and Stolterfoht *et al.* [18] reported transmission in the very beginning of charge-up, at the expected first patch angles. In addition, the aspect ratio of the capillaries used in the experiments of Kanai *et al.* [17] and Stolterfoht *et al.* [18] are much smaller (60) than ours (250). The geometrical opening angle for ions deflected from the entrance patch in Ref. [17] is as large as 1.4° at tilt angle 2.8°, while, in our case, it is only 0.26° at tilt angle -2°. It is reasonable that the lower beam energy and therefore lower transverse energy requires less charge on the first patch for deflection of the ions in the very beginning of charging-up, and this also makes it possible to observe the initially deflected ions. Also, the model calculations show that for only an entrance charge patch ($\varphi_0 = -\pi$ and $n = 2$ set in U_φ), the resulting transmission rate is negligible. Instead, ions are either deposited directly at the entrance or deflected at angles leading to the formation of a second patch [Figs. 6(a) and 7].

2. The charge patches downstream of the entrance patch

After the turning point, the transmitted angular distribution shifts back toward the tilt angle [Figs. 4 and 6(c)]. Two scenarios can account for this reversed shift. One is the scenario described in the model calculation where the exit patch becomes more extended around the circumference of the capillary. The other scenario is a weakening of the middle and exit patch that results in guiding the ions along the capillary axis, as suggested in Ref. [18]. However, this contradicts the measured increase of the angular width (see Fig. 4). Stolterfoht *et al.* [18] proposed that charge patches downstream of the entrance patch would lose their significance for ion guiding in the stationary state of transmission. If this was the case, a decrease of angular width at the final stage of charge-up would be seen due to the stronger collimation by the capillary wall. They did not observe such an evolution of the angular width [18]. We investigated also the significance of the charge patches beyond the entrance by a discharging and subsequent recharging measurement [16]. If both the exit patch and the middle patch lost their locality when the stationary state of transmission is reached, then, first, the transmitted ions would not emerge at angles ranging from the tilt angle -2° to a smaller deflection angle, -1.8°, i.e., closer to the incident beam direction during discharging [16]. Second, during recharging, the formation of the charge patches downstream of the entrance patch would again lead to a turning point in the shifting angular distributions [16]. Therefore, all charge patches are rather well localized in the stationary state of transmission.

In our case of 7-keV Ne^{7+} at tilt angle -2°, three patches are needed to account for shifts of the angular distributions in the charge-up process and at the stationary state of transmission. A larger number of patches in the latter half of the capillaries would imply that there are more turning points in the shift of the angular distribution, which is not seen in the experiment. Hence, a formation with other than three charge patches cannot be possible under the given conditions. Kanai *et al.* [17] reported that there are two patches, an entrance patch and a secondary patch, for 3.5- and 4.9-keV Ne^{7+} ions at the tilt angle 2.8°. At higher energy, 7 keV, they suggest that there is no charge patch in addition to the entrance patch. However, we find that only one entrance patch is not enough to account for the center of the angular distribution at smaller deflection angles ($\approx 1.5^\circ$), for 7-keV Ne^{7+} in the beginning of charging-up in the case of Ref. [17]. Since many factors differ, i.e., the tilt angle, dimensions of the capillaries, the kinetic energy, and the material properties, the exact number of charge patches for any given experiment can, however, be expected to vary [16–18].

D. Initially discharged capillaries: Broadening of transmitted angular distributions

As the measured widths are often wider than expected from the experimental parameters [8], it was proposed that there may be a broadening effect from the defocusing due to the exit field of an entire ensemble of nanocapillaries [11,20]. The analytic expression for the exit field can be found in Ref. [11]. It was derived by seeing the ensemble of capillaries as a condenser. For a single capillary this exit field has cylinder symmetry with respect to the capillary axis and is independent on the φ direction of the capillary in cylindrical coordinates (see Fig. 5). Therefore, the defocusing effect will have no φ dependence. The broadening due to this exit field should be isotropic—in both the ϕ plane and θ plane. The additional angular spread due to the exit field can be estimated by the transverse velocity gained by ions passing the exit. We simply consider the case of a trajectory being parallel to and within the distance $\rho = a/2$ from the capillary axis. In this case, the maximum angular spread of a trajectory at the distance $\rho = a/2$, parallel to the capillary axis, due to the defocusing of the exit field is calculated to be less than 0.01° for the case of 7-keV Ne^{7+} transmitted through SiO_2 nanocapillaries at the tilt angle -2°; even if all the incident charge into a capillary is accumulated at the entrance. This is much smaller than the maximum angular spread of $\sim 0.71^\circ$ at the limit of the dc dielectric breakdown strength. Therefore, the broadening effect from the defocusing due to the exit field is negligible in our case.

We find an appreciable broadening of the transmitted angular distributions only in the ϕ plane but not in the θ plane during charge-up in the case of initially fully discharged capillaries (see Fig. 2 in Ref. [16]). The formation and growth of the charge patches downstream of the entrance patch leads to a broadening in the ϕ plane and results in an increase of the angular width. This important aspect was not considered in the discussions of Kanai *et al.* [17] and of Stolterfoht *et al.* [18].

E. Already-charged capillaries: Charge pattern for the angular structure

The evolution of the angular distributions of ions transmitted through capillaries that were previously charged-up at a different tilt angle reflects the rearrangement of charge patches inside the capillaries. The capillary keeps a "memory" from the previous tilt angle after the change to a different one. We have derived a charge pattern of three patches guiding ions in the stationary state of transmission at tilt angle 2°. This gives the initial charge pattern for the already-charged capillaries before rotating from $+2^\circ$ to $+1^\circ$. At the tilt angle of 1°, a fraction of 21% of the capillary length is exposed to the incident beam, and for the tilt angle 2°, 10% is exposed. The transverse energy of ions entering the capillary is 2.1 eV at 1° and 8.5 eV at 2°. The increase of the exposed length and decrease of the transverse energy of ions in going from $+2^\circ$ to $+1^\circ$ will make a difference for ions hitting the capillary wall at different distances from the entrance charge patch. One group of ions will be guided directly from the entrance patch to the exit (peak 1 in Fig. 3), whereas another group will be deflected by the remaining patches downstream of the entrance patch and exit the capillary at the previous tilt angle $+2^\circ$ (peak 2 in Fig. 3). Therefore, the first peak is from the forming charge patches at the changed tilt angle $+1^\circ$, while the second peak can be attributed to the old charge patches from the "memory" of the previous tilt angle $+2^\circ$. Due to the relaxation of the old charge patches, the second peak shrinks and shifts toward the first peak centering on the new orientation of the capillary axes. During the formation of the new charge patches, the first peak grows and shifts to the angle around the new orientation of the capillary axes. The rearrangement of charge patches at the changed tilt angle is much faster

than discharging the capillaries, i.e., around 30 min for the rearrangement compared to the discharge time in the order of 10^3 min [16]. This suggests that the charge relaxation inside the capillaries can be driven by the incident charges. This can be associated with the Frenkel-Poole process [15,25]. The discharge current can increase as the electric field increases, due to the accumulation of deposited charge from the incident ions.

F. Scaling law

A scaling law for capillary guiding has been established [21,22]. This scaling law shows the relation between $\sin^{-2}\psi_c$ and E_p/q (E_p is the projectile energy) by introducing a characteristic tilt angle ψ_c. This characteristic tilt angle is defined as the angle at which the experimental fraction of transmitted ions falls to $1/e$ when a Gaussian exponential decay function is used to account for the transmission fraction as a function of tilt angles [22]. Here we show a connection of the scaling law with the model potential described above.

The ions can be deflected toward the direction of the capillaries if the transverse velocity of the ions goes to zero during the passage of the entrance patch region. Therefore, we have a critical tilt angle ψ_c, above which ion transmission cannot be discerned, that satisfies the relation

$$\frac{F_0 q}{m}\frac{\frac{D}{\tan\psi_c}}{\sqrt{\frac{2E_p\cos^2\psi_c}{m}}} = \sqrt{\frac{2E_p\sin^2\psi_c}{m}}, \tag{2}$$

where F_0 is the transverse component of the electric field and D is the diameter of the capillary. If an approximate electric field $F_0 = (1-\frac{1}{e})\frac{U_z|_{\text{entrance}}}{D/2}$ from the radial part of the model potential is inserted in Eq. (2), we have a relation between ψ_c and E_p/q as follows:

$$\sin^2\psi_c = \left(1-\frac{1}{e}\right)\frac{U_z|_{\text{entrance}}}{E_p/q}. \tag{3}$$

The above relation of $\sin^{-2}\psi_c$ and E_p/q for a fixed $U_z|_{\text{entrance}}$ agrees with the scaling law of capillary guiding as suggested in Refs. [21,22]. This similarity is attributed to the well-known fact that E_p/q is a common scaling parameter for ion trajectories governed by electrostatic fields. The low transmission rate $\sim$0.01% at the tilt angle -4° (after an incident charge of 1593 e/capillary) can be regarded as the tilt angle limit for transmission from our measurement and we can derive an upper limit of the potential $U_z|_{\text{entrance}} = 7.7$ V by inserting $\psi_c = 4^\circ$ to Eq. (3). As shown, the upper limit for the guiding angle ψ_c can be characterized by $U_z|_{\text{entrance}}$ for a beam of certain energy and charge state. $U_z|_{\text{entrance}}$ represents a capacity of the amount of charges collected on the inner surface at the entrance, which depends on the electrical properties of the capillaries.

V. SUMMARY AND CONCLUSIONS

Time evolution of the angular distribution of ions transmitted through SiO_2 nanocapillaries has been measured under defined initial conditions: already-charged, as well as fully discharged, capillaries. For fully discharged capillaries, we derived distinct charge patterns for three stages in the charge-up process, with the help of a model calculation. In the early stage of charge-up, the formation of the second patch downstream of the entrance patch leads to the smaller deflection angles for the transmitted ions, i.e., closer to the beam direction. The formation of the third patch, close to the exit results in the shift of the transmitted angular distributions to the larger deflection angles, i.e., away from the beam direction. In the stationary state of transmission, the exit patch becomes extended around the circumference of the capillary. The deposited charge patches, formed during charge-up, remain localized in the stationary state of ion transmission. For the already-charged capillaries, after rotation by one degree, the charge patches from previous exposure together with the forming charge patches lead to a transient double peak in the transmitted angular distribution. The rearrangement of the charge patches is much faster than their discharge, suggesting that the charge relaxation inside the capillaries can be driven by the incident charges, such as in a Frenkel-Poole process.

ACKNOWLEDGMENTS

We are grateful for helpful discussions with Klaus Schiessl (TUW, Vienna). We also thank Daniel Fischer (MPI, Heidelberg), for his help with the detection and acquisition system. We thank the staff of the Manne Siegbahn Laboratory for providing the beam. This work was financially supported by the European network ITS-LEIF and by VR.

[1] Y. Yamazaki, Phys. Scr. T **73**, 293 (1997).
[2] S. Ninomiya, Y. Yamazaki, F. Koike, H. Masuda, K. Komaki, K. Kuroki, and M. Sekiguchi, Phys. Rev. Lett. **78**, 4557 (1997).
[3] K. Tökési, L. Wirtz, C. Lemell, and J. Burgdörfer, Phys. Rev. A **61**, 020901 (2000).
[4] A. Arnau *et al.*, Surf. Sci. Rep. **27**, 113 (1997).
[5] N. Stolterfoht, J.-H. Bremer, V. Hoffmann, R. Hellhammer, D. Fink, A. Petrov, and B. Sulik, Phys. Rev. Lett. **88**, 133201 (2002).
[6] R. Hellhammer, Z. D. Pesic, P. Sobocinski, D. Fink, J. Bundesmann, and N. Stolterfoht, Nucl. Instrum. Methods B **233**, 213 (2005).
[7] Gy. Víkor, R. T. Rajendra Kumar, Z. D. Pešič, N. Stolterfoht, and R. Schuch, Nucl. Instrum. Methods B **233**, 218 (2005).
[8] M. B. Sahana, P. Skog, Gy. Vikor, R. T. Rajendra Kumar, and R. Schuch, Phys. Rev. A **73**, 040901(R) (2006).
[9] S. Mátéfi-Tempfli *et al.*, Nanotechnology **17**, 3915 (2006).
[10] P. Skog, I. L. Soroka, A. Johansson, and R. Schuch, Nucl. Instrum. Methods B **258**, 145 (2007).
[11] K. Schiessl, W. Palfinger, K. Tokesi, H. Nowotny, C. Lemell, and J. Burgdörfer, Phys. Rev. A **72**, 062902 (2005).
[12] T. Ikeda, Y. Kanai, T. M. Kojima, Y. Iwai, T. Kambara, Y. Yamazaki, M. Hoshino, T. Nebiki, and T. Narusawa, Appl. Phys. Lett. **89**, 163502 (2006).
[13] A. S. El-Said *et al.*, Phys. Rev. Lett. **100**, 237601 (2008).

[14] Y. Iwai, T. Ikeda, T. M. Kojima, Y. Yamazaki, K. Maeshima, N. Imamoto, T. Kobayashi, T. Nebiki, T. Narusawa, and G. P. Pokhil, Appl. Phys. Lett. **92**, 023509 (2008).

[15] N. Stolterfoht, R. Hellhammer, J. Bundesmann, D. Fink, Y. Kanai, M. Hoshino, T. Kambara, T. Ikeda, and Y. Yamazaki, Phys. Rev. A **76**, 022712 (2007).

[16] P. Skog, H. Q. Zhang, and R. Schuch, Phys. Rev. Lett. **101**, 223202 (2008).

[17] Y. Kanai, M. Hoshino, T. Kambara, T. Ikeda, R. Hellhammer, N. Stolterfoht, and Y. Yamazaki, Phys. Rev. A **79**, 012711 (2009).

[18] N. Stolterfoht, R. Hellhammer, D. Fink, B. Sulik, Z. Juhász, E. Bodewits, H. M. Dang, and R. Hoekstra, Phys. Rev. A **79**, 022901 (2009).

[19] R. T. R. Kumar, X. Badel, G. Vikor, J. Linnros, and R. Schuch, Nanotechnology **16**, 1697 (2005).

[20] K. Schiessl, W. Palfinger, K. Tőkési, H. Nowotny, C. Lemell, and J. Burgdörfer, Nucl. Instrum. Methods B **258**, 150 (2007).

[21] R. Hellhammer, J. Bundesmann, D. Fink, and N. Stolterfoht, Nucl. Instrum. Methods B **258**, 159 (2007).

[22] N. Stolterfoht, R. Hellhammer, J. Bundesmann, and D. Fink, Phys. Rev. A **77**, 032905 (2008).

[23] K. Schiessl (private communication).

[24] E. Harari, J. Appl. Phys. **49**, 2478 (1978); N. Klein and H. Gafni, IEEE Trans. Electron Devices **13**, 281 (1966).

[25] J. Frenkel, Phys. Rev. **54**, 647 (1938).